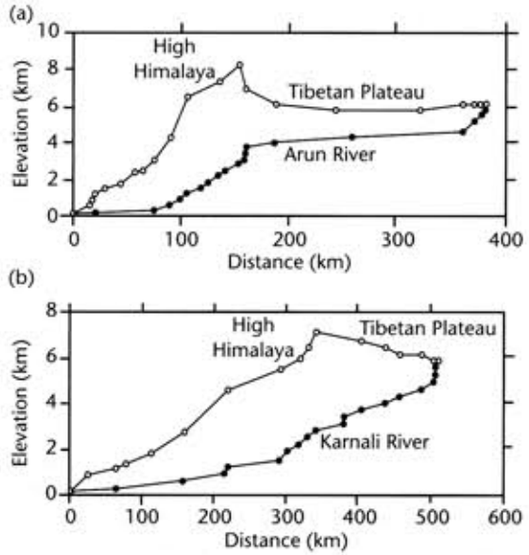

Fig. 7.21 Long profiles of the mountain peaks and valley bottoms along the Arun (a) and Karnali (b) rivers, showing the high elevation of the summits c. $x = 200$ km from the headwater regions, suggesting that bedrock river incision rates produce an isostatic uplift of the peaks. After Montgomery (1994). Reproduced courtesy of American Geophysical Union.

7.5.3 Long range fluvial transport

A fundamental characteristic of alluvial channels is that they have sufficient sediment to equal or exceed the transport capacity. The transport of sediment in river systems has been the subject of modeling by a generation of civil engineers, geomorphologists, and latterly, geologists. Our purpose here is not to attempt a full description of long range sediment transport by rivers. For more comprehensive treatments the reader is referred to Parker (1978a, b), Paola et al. (1992) and Dade and Friend (1998).

Various forms of diffusion equation of the type given in equation (7.24) have been applied to long range fluvial transport. Here we concentrate on an assessment of long range fluvial transport of a mixture of gravel and sand. The quantitative development of this group of models can be found in Paola et al. (1992) and Marr et al. (2000). It is well known in modern mixed gravel–sand fluvial systems that there is a relatively steep gravelly proximal zone with an abrupt change to a lower gradient sandy zone (Sambrook-Smith and Ferguson 1995). To be able to predict the movement of the "gravel front," or "gravel–sand transition" would be of considerable benefit in basin analysis.

Most models of sediment transport in rivers make the same set of assumptions.

1 First, it is assumed that the long term flow of water in a river approximates that of a steady uniform flow down an inclined plane. For a flow of depth h and density ρ on a slope $\delta y/\delta x$, the downslope component of the fluid weight on a unit area of the river bed is $\rho gh\delta y/\delta x$. This downslope acting force must be opposed by an equal and opposite drag force exerted on the fluid by the unit area of bed – this is the shear stress τ_0 (Fig. 7.22a). Consequently, the force balance gives

$$\tau_0 = -\rho gh\frac{\partial y}{\partial x} \tag{7.37}$$

Rivers are anything but steady and uniform. However, equation (7.37) can be used as an approximation for long-term river behavior. It works best for shallow high-gradient streams and worst for deep, low-gradient streams. If the flow depth is large compared to the channel width, h should be replaced by the *hydraulic radius* R in equation (7.37) (Fig. 7.22b).

2 Second, we make use of an equation that expresses the resistance to flow in the channel. A fluid moving over its bed and banks experiences frictional losses of energy known as *flow resistance*. Where the bed of the river is rough, as is always the case in natural rivers, the energy losses should in some way be related to the length scale of the roughness of the bed. This roughness can be expressed in a number of ways. A common method is to use the *Darcy–Weisbach friction factor* f

$$f = \frac{8\tau_0}{\rho_f u^2} \tag{7.38}$$

where u is the flow velocity. The friction factor (or similar forms such as the Chézy coefficient C and Manning's n) varies strongly according to the grain size of the sediment on the river bed and is especially affected by the presence of bedforms such as ripples and dunes and of macroforms such as bars, chutes, and pools.

3 Third, we conserve the discharge of water through the system. Consider a slice of width B of an alluvial basin of length L, which has active channels on its surface with cumulative width b, of flow depth h and containing flows of velocity u (Fig. 7.23). Let β be the fraction of the section width B occupied by channels, so $\beta = b/B$. The discharge of water Q_w in the channels occupying the width of floodplain B is bhu, or averaged across the floodplain is βhu. Consequently,

$$\beta = \frac{Q_w}{hu} \tag{7.39}$$

4 Finally, we make use of the sediment continuity equation (7.16), modified by the use of a dimensionless shear stress τ_*, as given by Shields

$$\tau_* = \frac{\tau_0}{(\rho_s - \rho_f)gD} \tag{7.40}$$

where D is the median grain size and ρ_s and ρ_f are the sediment and fluid densities respectively. There appear to be strong limits on the value of the dimensionless shear stress, so that it can be treated as a constant, at about 1.4 times the critical shear stress at the threshold of particle motion in coarse-grained braided rivers, and between 1 and 2 in alluvial sand-bed rivers (Paola and Seal 1995; Dade and Friend 1998; Parker et al. 1998). It is probably a constant because if it is too high, the stream erodes its banks and widens its bed, thereby reducing the shear

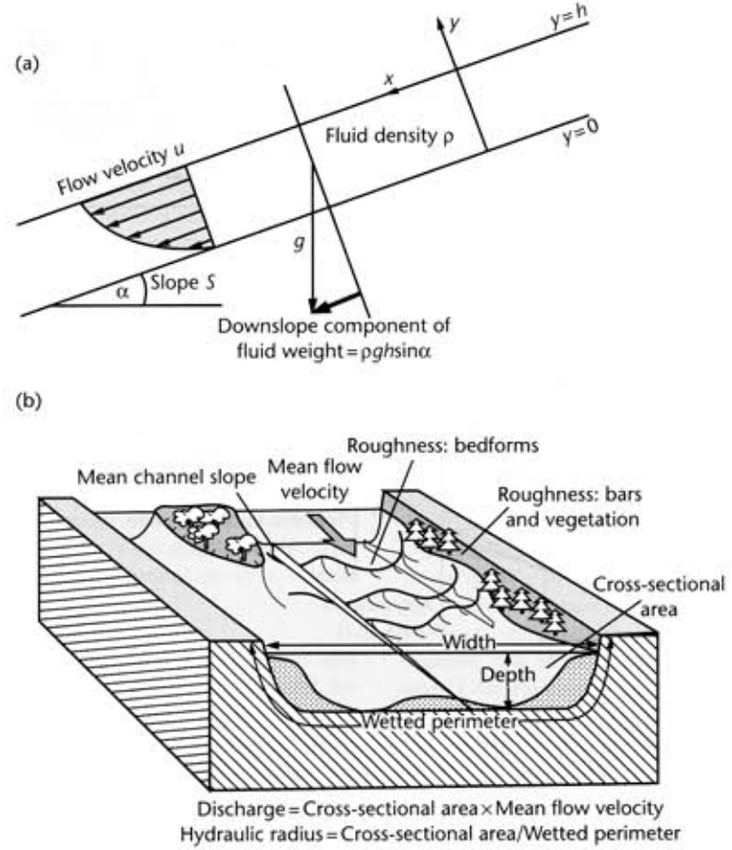

Fig. 7.22 (a) Notation for steady uniform flow down an inclined plane of slope $\sin\alpha$; (b) The wetted perimeter and hydraulic radius of a river. The presence of bar forms, pools, dunes and ripples, vegetation, and pebbles all contribute to the friction factor of the river.

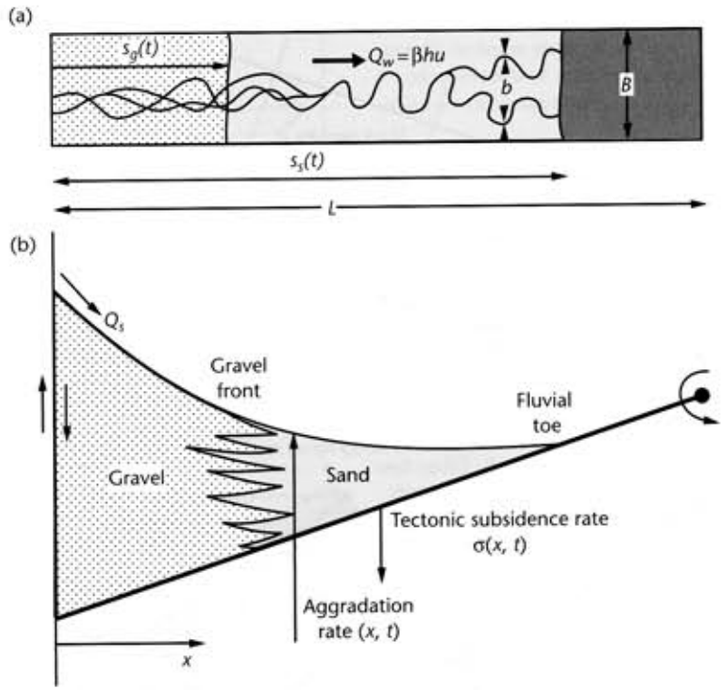

Fig. 7.23 Map view and cross-section of a slice of alluvial basin of length L, width B, containing channels with cumulative width b undergoing tectonic subsidence $\sigma(x)$ approximated by a linear tilt from a distant hinge. Note the break in slope at the gravel front and the position of the fluvial toe. After Marr et al. (2000). Reproduced courtesy of Blackwell Publishing Ltd.

stress per unit area of stream bed (Parker 1978a, b). There is a sharp jump in τ_* at the gravel–sand transition or "gravel front" in many rivers The modified sediment continuity equation therefore has the form

$$\frac{\partial y}{\partial t} = \frac{\partial}{\partial x}\left(\kappa \frac{\partial y}{\partial x}\right) - \sigma(x) \tag{7.41}$$

where the effective diffusivity or transport coefficient κ of the alluvial system is dependent principally on the discharge of water, a friction (flow resistance) factor, a dimensionless sediment transport rate, and the dimensionless shear stress. The transport coefficient is constant within the gravel and sand regimes, but changes by a factor of about 10 at the boundary. Typical values for κ used by Marr et al. (2000) are 0.01 $km^2 yr^{-1}$ in the gravel regime and 0.1 $km^2 yr^{-1}$ in the sand regime.

The simplest approximation of the time required for equilibrium to be achieved with a set of forcing conditions, or *basin response time* T_{eq}, is L^2/κ, where L is the basin length, as in the diffusional problems previously encountered. In a two-diffusion model, the gravel and sand regimes may have their own response times. For a basin length of 100 km and κ for gravel of 0.01 $km^2 yr^{-1}$, the response time is 10^6 yr, whereas with κ for sand, we have a response time of 10^5 yr. An important parameter should be the period of the forcing T compared to the basin response time T_{eq}. Marr et al. (2000) considered cross-sections of basin stratigraphy under different conditions of forcing, using the total sediment flux Q_s, the water discharge Q_w, the gravel fraction f_g, and the rate of tectonic subsidence σ. When the forcing variable has a rapid sinusoidal change (for example, in sediment supply), $T \ll T_{eq}$, the time for equilibrium to be re-established is almost constant for a fixed gravel fraction, suggesting that the basin response time is controlled by the fluvial system rather than the frequency of the forcing. The value of this *intrinsic* response time is determined by the gravel fraction (fast – $<10^5$ yr – with low gravel fractions and slow – 10^5–10^6 yr – for high gravel fractions). In the simulations found in Figures 7.24 and 7.25, slow forcing is $T = 10^7$ yr, whereas fast forcing is $T = 10^5$ yr. The important aspects for basin analysis are as follows.

With *slow forcing* (Fig. 7.24):

1 The movements of the sand toe and gravel front are in phase with variations in sediment flux, with proximal and distal accumulation of sediment both occurring at the time of high sediment flux. Retreat of the fluvial toe at times of low sediment flux produces distal unconformities.
2 During periods of increased subsidence, sediment is trapped in proximal regions and distal areas are starved, causing a retreat of both the gravel front and the fluvial toe and the creation of distal unconformities. During periods of reduced subsidence rate, the gravel front and fluvial toe prograde since accommodation is reduced. Both proximal and distal accumulation are therefore out of phase with subsidence rate.
3 The position of the gravel front moves outwards when the gravel percentage (for a constant sediment flux) increases, producing a coarsening up in a vertical section.

For *rapid forcing* (Fig. 7.25):

1 Rapid changes in sediment flux produce gravel and sand regions with markedly different slopes, and the position of the gravel front is out of phase with the forcing. Reduced sediment supply causes a reduction in proximal slopes, the cutting of proximal unconformities and the progradation of the gravel front. In contrast, reduced sediment supply causes the fluvial toe to retreat. During periods of increased sediment supply, proximal slopes increase, which causes the gravel front to retreat, while the fluvial toe progrades slightly.
2 Rapid variations in subsidence rate have little effect on the gravel front.
3 The position of the gravel front and proximal accumulation are in phase with the percentage gravel fraction.

It is clear therefore that the stratigraphy of an alluvial system exhibits a complex response to the various forcing mechanisms. The response of the system depends on the time scale of the forcing compared to the basin response time T/T_{eq}. Proximal and distal unconformities, variations in proximal and distal accumulation and movements of the gravel front and fluvial toe may be in phase or out of phase with external forcing.

The response times of alluvial systems have also been approximated from measurements of the sediment discharge leaving the catchment. River basins may have extensive floodplain areas in their downstream portions, which act as buffers to changes in any forcing variables, such as base level change at a river mouth, or changes in sediment flux near their headwaters, and therefore may have long response times. If the system is assumed to be diffusive in character, and the discharge of water varies systematically with floodplain width W, the mass effective diffusivity κ of the channel–floodplain system is

$$\kappa = \frac{Q_s}{W\left\langle \frac{\partial y}{\partial x} \right\rangle} \tag{7.42}$$

where Q_s is the sediment discharge and < > denotes the spatial average of the slope. If L is the downstream length of the river–floodplain system and H the maximum relief between its upstream and downstream ends, the response time becomes

$$\tau = \frac{L^2}{\kappa} = \frac{L^2 W \langle \partial y/\partial x \rangle}{Q_s} = \frac{LWH}{Q_s} \tag{7.43}$$

The large river systems of Asia have typical values of $L \sim 10^6$ m, $W \sim 10^5$ m, $H \sim 1$–2×10^2 m (slopes of 10^{-3} to 10^{-4}), and sediment discharges Q_s of $10^{7\text{–}8}$ $m^3 yr^{-1}$ (Métivier and Gaudemer 1999). The characteristic response time is therefore in the region of 10^5 to 10^6 years. Castelltort and Van Den Driessche (2003) carried out a similar analysis on 93 of the world's major rivers, and found that response times varied between 10^4 yr to more than 10^6 yr. (Fig. 7.26). The response time depends on the scale of the channel–floodplain system. As we saw in the forward modeling of alluvial stratigraphy above, large alluvial systems therefore strongly buffer any variations in sediment supply with frequencies of less than $10^{5\text{–}6}$ years. This has strong implications for the detection of high frequency driving mechanisms in the stratigraphy of sedimentary basins.

7.5.4 Some aspects of numerical landscape evolution models

The numerical modeling of landscapes has developed over the last couple of decades. The significance of numerical landscape evolution for basin analysis is that such models allow the sediment supply to basins to be simulated in terms of tectonic, climatic, and geomorphic sets of rules. The incorporation into a physically realistic numerical model of feedbacks between the various processes that shape a landscape also allows system behavior, such as the response time to a change in a

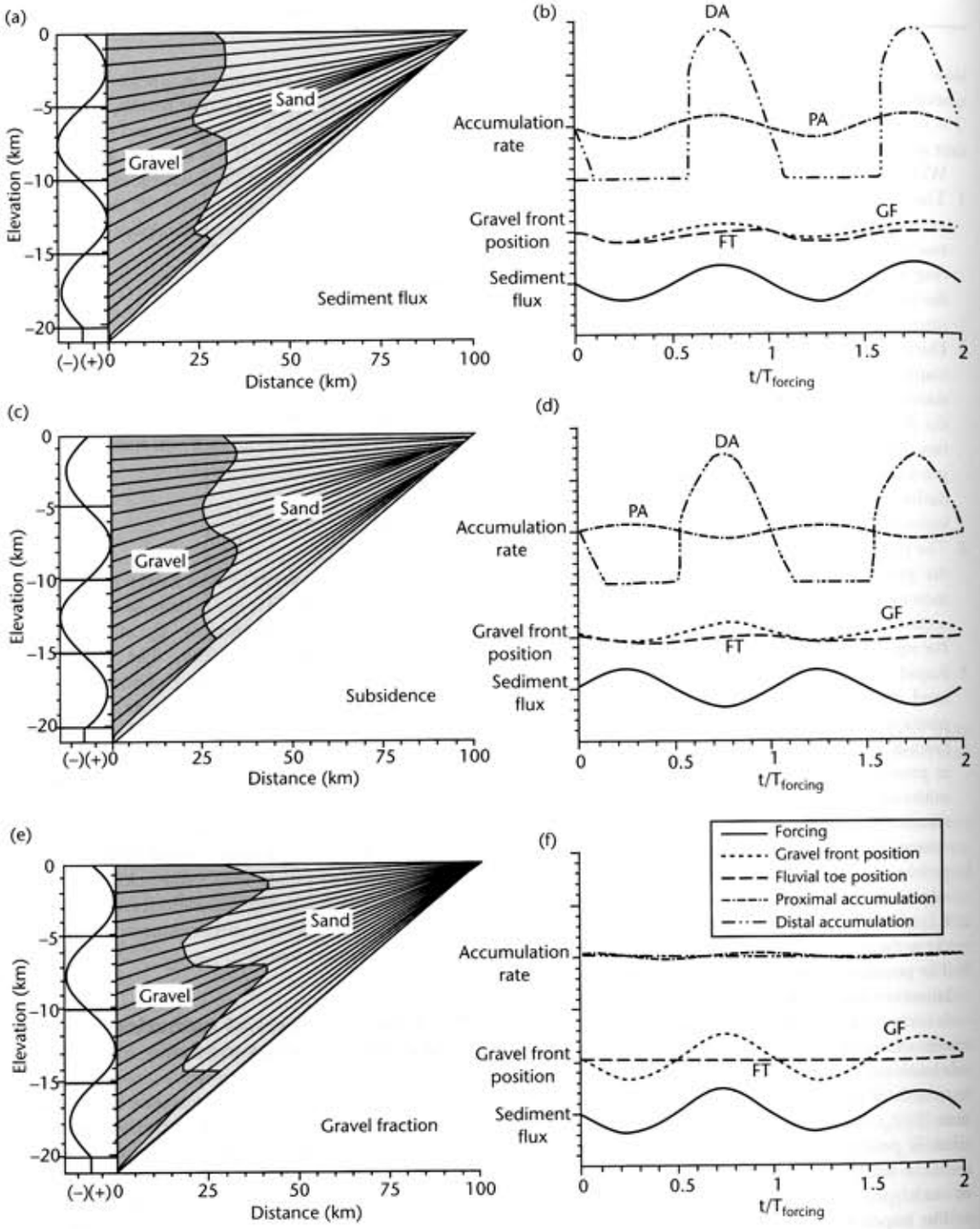

Fig. 7.24 Cross-sections of alluvial stratigraphy under slow sinusoidal forcing ($T > T_s$) of sediment flux (a), tectonic subsidence (c) and gravel fraction (e). Diagrams on right (b, d, f) show time variation of the position of the gravel front and fluvial toe, proximal and distal accumulation and the forcing variable. Further details can be found in Marr et al. (2000). GF, gravel front; FT, fluvial toe; DA, distal accumulation; PA, proximal accumulation. Reproduced courtesy of Blackwell Publishing Ltd.

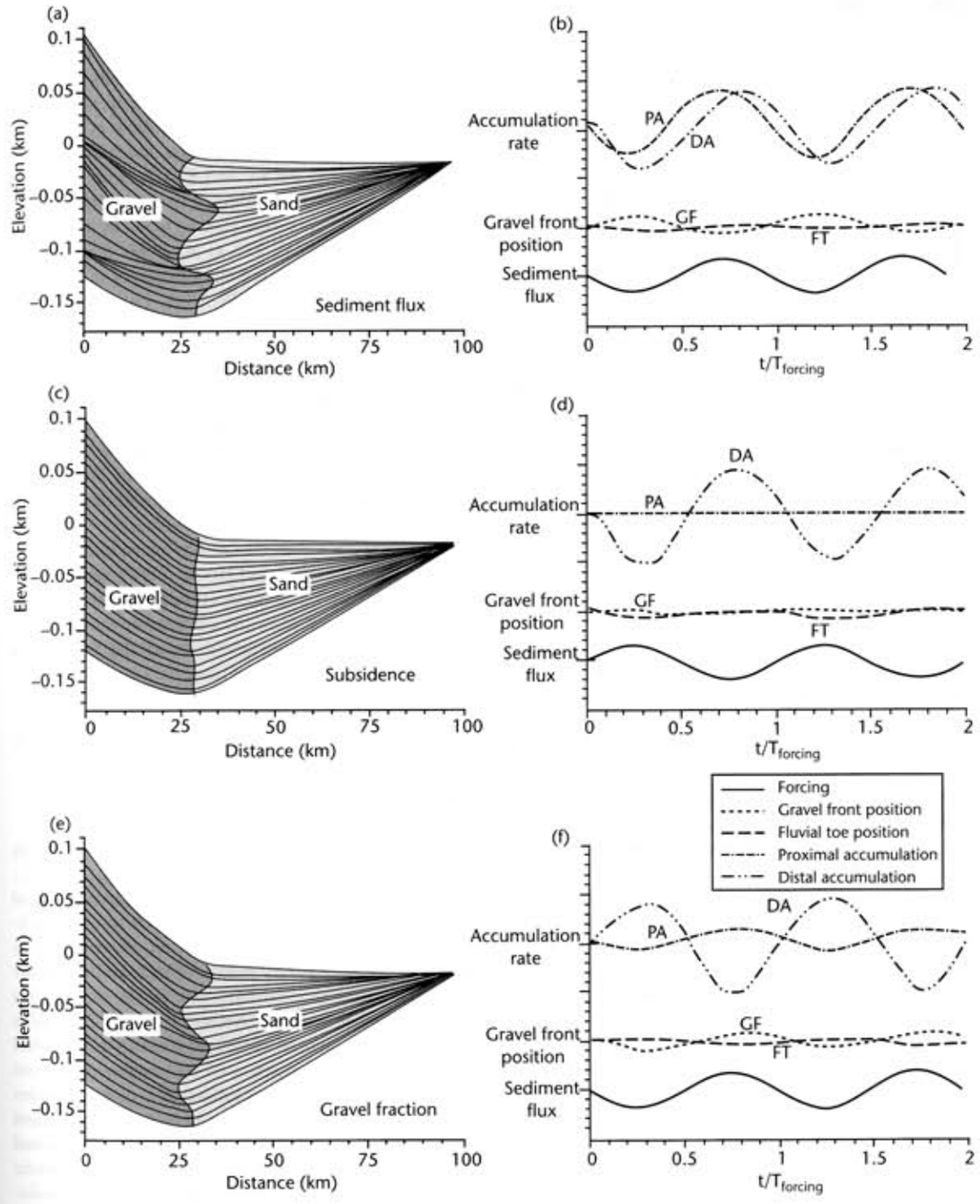

Fig. 7.25 Cross-sections of alluvial stratigraphy under fast sinusoidal forcing ($T < T_s$) of sediment flux (a), tectonic subsidence (c), and gravel fraction (e). Diagrams on right (b, d, f) show time variation of the position of the gravel front and fluvial toe, proximal and distal accumulation and the forcing variable. Further details can be found in Marr et al. (2000). Reproduced courtesy of Blackwell Publishing Ltd.

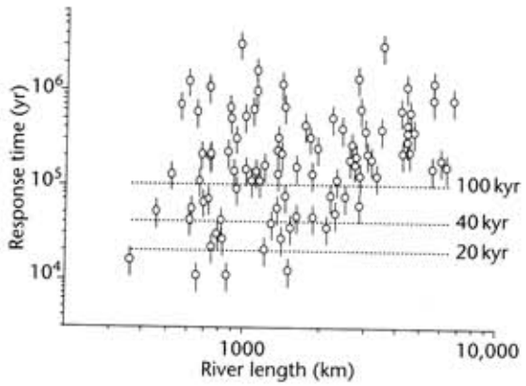

Fig. 7.26 Response times of some modern drainage basins, from a dataset compiled by Castelltort and Van Den Driessche (2003) using the relations given in equations (7.42) and (7.43). Hydrologic and geomorphologic data from Hovius (1998). Response time is plotted against river length. Vertical bars show uncertainties based on the unknown bedload sediment transport rates of the rivers shown. Note that the majority of response times are $>10^3$ yr, and some are $>10^6$ yr. Reproduced courtesy of Elsevier.

driving mechanism or forcing variable, to be studied. Numerical landscape models range in their spatial and temporal scales, from whole contractional orogens and passive margin mega-escarpments (length scales of *c.* 100 km and time scales of *c.* 10^7 yr) to individual extensional fault blocks or thrust-related anticlines (length scales of *c.* 10 km, time scales of *c.* 10^6 yr), and even to the fault scarps generated by single seismic events (length scale of *c.* 100 m, time scales of 10^3–10^5 yr). The resolution (of the elevation of topography) required by the landscape evolution model varies accordingly, from cm in the case of a degrading fault scarp, to *c.* 100 m for an orogen. The spatial and temporal scale and topographic resolution commonly affect the way in which tectonic and geomorphic processes are dealt with in the numerical model. Burbank and Anderson (2001) provide a useful summary. Many of the algorithms used in numerical landscape models are identical to or similar to those given in §7.5.1–§7.5.3. We concentrate here on the intermediate scale of extensional fault blocks and anticlinal folds in fold–thrust belts.

7.5.4.1 Tilted extensional fault blocks and thrust-related anticlines

Early attempts to model the evolution of simple fault-bounded ranges used a single planar fault with uniform slip, diffusional modification of the tectonically generated topography using a single, constant value of κ, and flexural compensation (King et al. 1988; Stein et al. 1988). Later models incorporated channels and hillslopes that strongly interacted (§7.5.1 and §7.5.2), with transport rules for the disposal of sediment derived from hillslope erosion, and hillslopes were allowed to fail by landsliding (Densmore et al. 1998; Ellis et al. 1999). Such models not only simulated very realistic landscapes in the Basin and Range Province of SW USA, but also allowed system behavior to be better evaluated. These tectonic–geomorphic systems involve steep transverse drainage systems over uplifting footwall blocks, with fans in the neighboring hangingwall basins (Whipple and Trayler 1996; Allen and Hovius 1998). The area of the catchment acting as a source terrain for sediment A_1, relative to that of the hangingwall fan A_2, is an indicator of how this relatively simple tectonic–geomorphic system functions (Fig. 7.27).

We introduce a dimensionless proportionality coefficient V, following Allen and Hovius (1998), which incorporates all the various processes resulting in the transport of sediment eroded from the catchment, routed to the fan head and then distributed across the fan with a spatially averaged deposition rate $\dot{y}$:

$$\phi = \frac{1}{\dot{y}} V \frac{(1-\lambda_r)}{(1-\lambda_f)} e_r e_f \tag{7.44}$$

and

$$A_1 = \phi A_2 \tag{7.45}$$

where V is the sediment efflux of the catchment, λ_r and λ_f are the porosities of rocks in the catchment and sediments on the fan respectively, e_r is an efficiency factor accounting for temporary storage of sediment within the catchment, and e_f is an efficiency factor allowing for escape of some sediment from the fan into down-fan sabkhas, lakes, or axial river systems. In the simplified case of complete evacuation of the catchment with no storage ($e_r = 1$) and a closed system for sediment delivery to the fan ($e_f = 1$), and assuming that rock and sediment porosities are comparable ($\lambda_r \equiv \lambda_f$), equations (7.44) and (7.45) simply illustrate that ϕ depends strongly on the rate at which the fan aggrades, which is controlled fundamentally by the rate of tectonically created accommodation. Consequently, tectonics play a major role in the creation of uplifting footwalls as source regions for sediment, in determining the spatial pattern and rate of hangingwall subsidence, and thereby in controlling fan

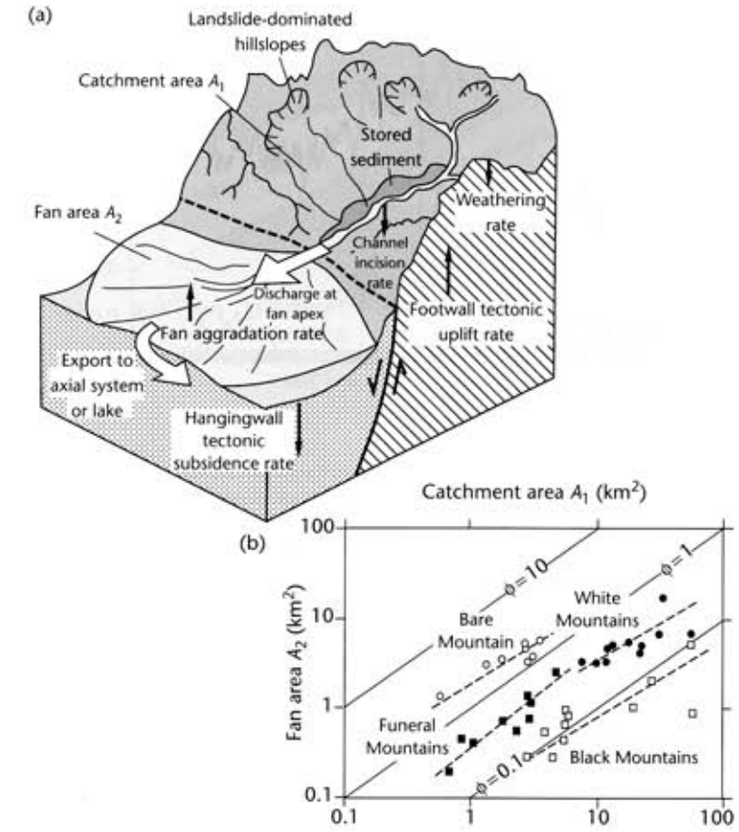

Fig. 7.27 (a) Schematic illustration of a catchment–fan system associated with a tilted extensional fault block (after Allen and Hovius 1998, Allen and Densmore 2000); (b) shows plot of catchment area A_1 versus fan area A_2 for catchment–fan systems in the arid southwestern US, showing that individual regions with particular slip rates are discriminated in terms of their value of ϕ.

thickness and fan progradation distance. Not surprisingly, plots of fan area versus catchment area from examples in the arid SW USA (Allen and Hovius 1998) show that areas with high fault displacement rates and areas with low fault displacement rates are discriminated by their value of ϕ (Fig. 7.27b). This implies that coarse-grained fan bodies are stacked against active range-bounding faults, whereas fans coalesce and prograde basinwards where fault displacement rates are smaller.

Using the landscape evolution model developed by Densmore et al. (1998), Allen and Densmore (2000) showed that abrupt changes in the rate of slip on range-bounding extensional faults could be recognized by changes in mean catchment erosion rate and mean fan deposition rate (Fig. 7.28), but that there was a delay in the achievement of a new steady state under the new fault slip rate conditions. This response time was *c.* 50 kyr for the catchment–fan systems in the Death Valley region of eastern California, regardless of climatic conditions. In other words, changes in the tectonic boundary conditions at a frequency of less than 50 kyr will be difficult to recognize in the stratigraphic record.

The deforming crustal template in regions of extension strongly interacts with erosion and drainage development. As footwalls emerge, river systems are etched into their flanks either side of a catchment divide. Individual *en echelon* fault segments interact at their tips in a variety of geometrical arrangements, most important of which is the *relay zone* (Larsen 1988). These relay zones are thought to have an important role in focusing

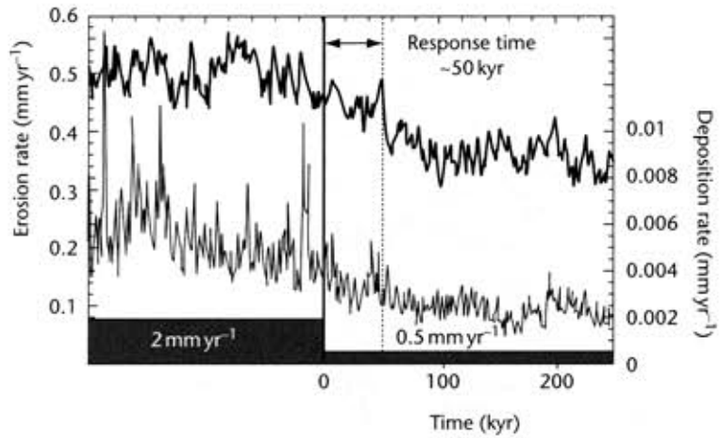

Fig. 7.28 Mean catchment-averaged erosion rate (heavy line) and mean fan deposition rate (thin line) before and after a step change in fault slip rate from 2 mm yr^{-1} to 0.5 mm yr^{-1}. Note the progressive decrease in erosion and deposition rates to new equilibrium values. The response times (the time required for each rate to fall to 1/e of its initial value) are 56 kyr for erosion rate and 48 kyr for deposition rate. After Allen and Densmore (2000). Reproduced courtesy of Blackwell Publishing Ltd.

sediment delivery to hangingwall basins from larger-than-normal catchments and are therefore thought to be associated with fan and fan–delta development (Leeder and Gawthorpe 1987; Gupta et al. 1999) (Fig. 7.29). Such sedimentary bodies adjacent to relay zones are potentially important as hydrocarbon reservoirs in rift provinces (§10.4). However, numerical landscape evolution models of fault systems under different histories of growth and linkage failed to produce large catchments and fans at relay zones (Densmore et al. 2003). This suggests that large catchment–fan systems at relay zones may be related to antecedent drainage rather than to local fault growth. Whereas the Basin and Range is typified by hydrologically closed footwall catchment systems, in which we do not expect to find large catchment–fan systems at relay zones, other extensional provinces may possess regional, antecedent drainages that deposit large fans at relay zone entry points into hangingwall depocenters, such as the southern Afar Rift, Gulf of Suez, and central Greece.

At a similar wavelength to the extensional fault blocks of the Basin and Range are the thrust-related folds of contractional tectonic provinces such as the Zagros of Iran and western Pakistan (Mann and Vita-Finzi 1988). Folds are *c.* 10 km in wavelength and 2–3 km in amplitude. There are a number of issues that are especially relevant to this tectonic situation: as hangingwall rocks are transported up the thrust ramp, how is the topographic profile and river drainage development related to the tectonic paths of hangingwall rocks? What is the effect of progressively unroofing rocks with markedly different erodibilities (or values of c_b or c_r)? And what effects do the contractional tectonics have on antecedent rivers?

In areas with high rates of tectonic uplift of rocks, the topographic relief is essentially controlled by the ratio U/c_r, where U is the tectonic uplift rate of rock and c_r is the efficiency of bedrock incision expressed as a velocity (eqn 7.35). Streams are known to change their gradients markedly over substrates of different erodibility (Hack 1973). Tucker and Slingerland (1996) estimated bedrock erodibilities c_r to vary from 0.02 m yr^{-1} to 0.2 m yr^{-1} in the arid landscapes of the Zagros. Using a numerical landscape evolution model, they successfully simulated the progressive unroofing of stratigraphy with strongly varying erodibility related to the growth of a series of tectonic folds. Sediment flux from the fold–thrust belt reflects both tectonic growth of the fold structures but also the extent of exposure of resistant versus weak lithologies. For a landscape dominated by bedrock channels, the time required to reach equilibrium (90% of equilibrium sediment flux) with a given rate of tectonic uplift is proportional to the rock erodibility c_r, the rock uplift rate U, and the spatial scale (width) of the uplifting rock region L,

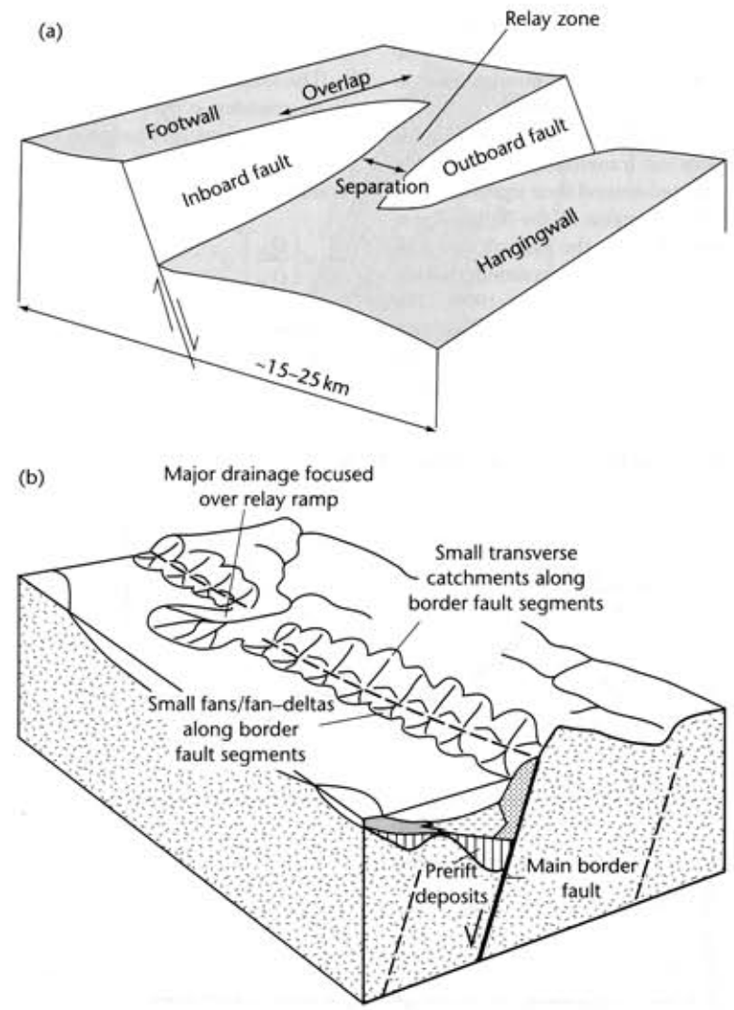

Fig. 7.29 (a) Perspective view of a soft-linked extensional relay zone; (b) Conventional view of relay zones as sites of large fan systems, whereas the main border faults have small transverse catchments and small fans/fan deltas.

$$\tau = k\frac{U^{\left(\frac{1-i}{n}\right)}L}{c_r^{1/n}} \qquad (7.46)$$

where n is the exponent for slope in equation (7.35), commonly assumed to be 2/3. Calibrated against model output from a landscape evolution model used to simulate the topography of the Zagros (using $c_r = 0.02$ to 0.2 m yr^{-1}, $L = 40$ km, and $U = 1$ mm yr^{-1}), the coefficient of proportionality k in (7.47) is 7–10. The geomorphic response time τ for sediment flux is between *c.* 0.1 Myr and 4 Myr for the weak and resistant lithologies respectively. For the resistant lithologies, the geomorphic response time is very long (>1 Myr). In this case, it is most likely that periods of different thrust displacement rate in the fold–thrust belt would not be discernible in the stratigraphic record of neighboring foreland and thrust-sheet-top basins. However, small thrust-related anticlines

composed of weak lithologies should respond quickly to changes in tectonic boundary conditions, and produce a recognizable pulse of sediment in the basin. Figure 7.30 shows the evolution of sediment flux through time as rocks with different erodibility are unroofed.

It is apparent from a casual inspection of topographic maps that some streams cut transversely through folds, whereas others are deflected around their tips (Fig. 7.31). For example, in the Marche region of the Italian Apennines, a series of rivers drain to the Adriatic coast by cutting straight through the points of maximum tectonic uplift in NW–SE oriented folds (Alvarez 1999). The impact of growing tectonic structures on drainage patterns has been discussed by a number of authors (Jolley et al. 1990; Burbank and Vergés 1994; Talling et al. 1995; Burbank et al. 1996; Gupta 1997). One of the major impacts for basin analysis is that sediment entry points into basins may be shifted by growing tectonic structures.

The simplest approach to understanding this problem is to consider a river that is in equilibrium between channel incision and tectonic uplift rates. For bedrock streams, we can modify equation (7.35) for the case of equilibrium to give

$$\frac{U}{\epsilon_r} = \left(\frac{Q_w}{Q_*}\right)^m S^n \tag{7.47}$$

If the uplift rate of rocks in the fold crest region is high ($U = 0.01\,\mathrm{m\,yr^{-1}}$) and the stratigraphy is strongly resistant ($\epsilon_r = 0.025\,\mathrm{m\,yr^{-1}}$), the dimensionless ratio U/ϵ_r is high

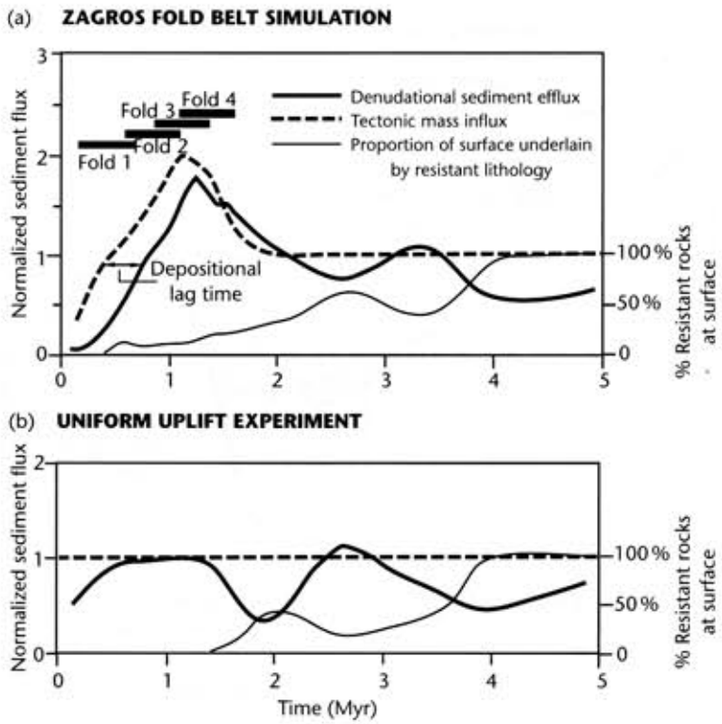

Fig. 7.30 Landscape evolution model results of the unroofing of folds in the Zagros fold–thrust belt. (a) Tectonic influx from uplift of rock (dashed line) and sediment efflux out of the model grid (solid line) versus time. In this simulation, four anticlinal folds grow progressively in time. Note the lag time between tectonic influx and depositional response of <0.5 Myr during the growth phase of the folds. The thin solid line shows the percentage of resistant rocks exposed at the land surface as a function of time. Note that the decrease then increase of sediment efflux is due to this variation in erodibility of outcropping rocks; (b) Sediment efflux in which the variations are solely due to lithological variations in the stratigraphy being unroofed. Tectonic influx is spatially and temporally uniform. After Tucker and Slingerland (1996). Reproduced courtesy of Blackwell Publishing Ltd.

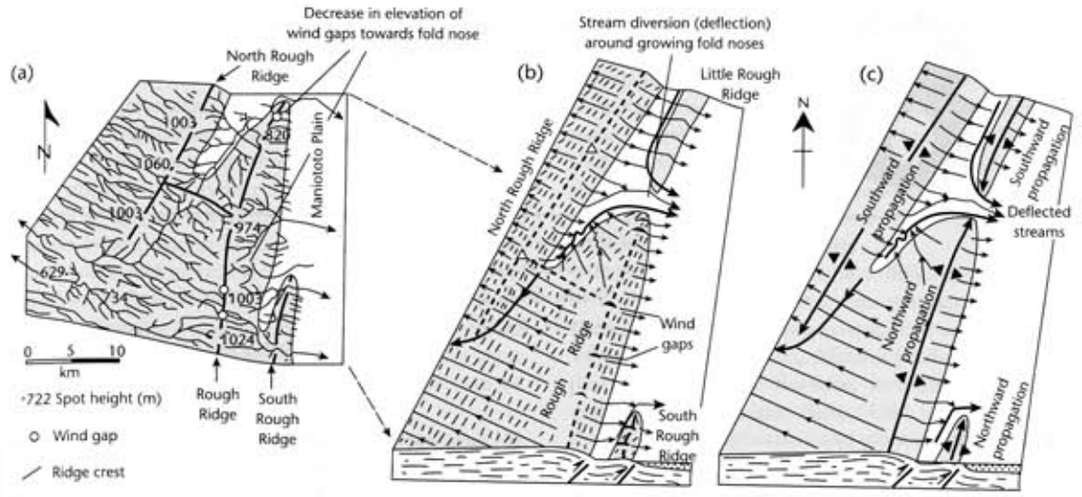

Fig. 7.31 Evolution of landscape in the face of growing folds, exemplified by the Southern Alps of central Otago, New Zealand (after Jackson et al. 1996). (a) Drainage network, fold crests, plunging fold noses, water gaps, wind gaps, and their elevations in the vicinity of Rough Ridge. Note the decrease in elevation of the wind gaps towards the fold nose; (b) Schematic diagram of drainage pattern, showing clear diversion of drainages around the nose of each growing fold; (c) Interpretation of fold propagation of same region of Rough Ridge and the resultant drainage development. Reproduced courtesy of Pergamon Press, Oxford.

(0.4), indicating that a stream is likely to be deflected. If, however, the uplift rate of rocks in the fold crest region is low ($U = 0.001\,\mathrm{m\,yr^{-1}}$) and the rocks are weakly resistant to erosion ($\epsilon_r = 0.25\,\mathrm{m\,yr^{-1}}$), U/ϵ_r is low (0.004), indicating that the discharge–slope product of the stream may be sufficient to cut through the growing anticline. As a growing fold emerges, the width of the fold should increase. Field studies (e.g., Burbank et al. 1996; Jackson et al. 1996) suggest that if the elevation of the entrance and exit of the fold are fixed, the widening of the fold may cause a decrease in stream gradient and stream power, leading to defeat of the stream by the growing structure (see eqn 7.47). Alternatively, aggradation upstream of the entrance to the fold may cause avulsion of the stream to a lower position of the floodplain, effectively diverting the stream away from the growing fold. Deflected (defeated) streams are commonly captured by adjacent streams, which increases their discharge, allowing them to incise through the growing fold. The interaction of river drainage, erosion, topography and tectonic displacements is currently a rich area of research.

Coupled tectonic–erosion models at the scale of whole orogens, discussed in §4.6 and §4.7, involve the description of the tectonic deformation of the lithosphere in zones of convergence, coupled with a surface landscape of hillslopes and active channels and depositional basins (Beaumont et al. 1992, 1996b; Willett et al. 1993; Kooi and Beaumont 1994, 1996). As we have seen (§4.7), orogenic wedges with an asymmetry of climate (precipitation) on windward and leeward flanks are associated with an asymmetry of exhumation of deep crustal rocks. A structurally much simpler situation at a similar spatial and temporal scale is provided by the classic mega-escarpments found along segments of passive margins (Gilchrist and Summerfield 1990). The high escarpments of southern India (Western Ghats) (Gunnell 1998), Namibia–South Africa (Gallagher and Brown 1999), and SE Australia (Seidl et al. 1996) are good examples. Landscape evolution models of passive margin mega-escarpments are found in Kooi and Beaumont (1994) and Braun and Sambridge (1997).